Synaptic Dysfunction and Compensation After NMDA Receptor Ablation in the Mouse Medial Prefrontal Cortex

Rachel M. Dick[1], Lydia B. Cunitz[2], Aurora Torres Pérez[3], Habsa Ahmed[2], Jason S. Mitchell[4], Ezequiel Marron Fernandez de Velasco[5], Nicola M. Grissom[6] & Patrick E. Rothwell[2*]

[1]Graduate Program in Neuroscience, University of Minnesota, Minneapolis, MN

[2]Department of Neuroscience, University of Minnesota, Minneapolis, MN

[3]University of Puerto Rico - Río Piedras, San Juan, PR

[4]Department of Microbiology and Immunology, University of Minnesota, Minneapolis, MN

[5]Department of Pharmacology, University of Minnesota, Minneapolis, MN

[6]Department of Psychology, University of Minnesota, Minneapolis, MN

*Corresponding Author:

Patrick E. Rothwell, Ph.D.
4-142 Wallin Medical Biosciences Building
2101 6th Street SE
Minneapolis, MN, 55455
Phone: 612-626-8744
Email: rothwell@umn.edu

ABSTRACT

The glutamate hypothesis of schizophrenia posits that patients' symptoms arise from abnormal corticolimbic glutamatergic signaling, which is supported by evidence of abnormal expression of N-methyl-D-aspartate receptors (NMDARs) and decreased dendritic spine density in the prefrontal cortex (PFC). Pharmacological blockade of NMDARs in humans and animal models induces psychotomimetic symptoms, cognitive deficits, and decreased neural synchrony, with genetic knockdown of NMDARs providing further evidence of altered spine density and synaptic transmission. However, it is unknown how chronic loss of NMDARs in the PFC during adolescence – a developmental time period associated with significant synaptic pruning and symptom onset in patients – affects spine density and neurotransmission, and whether compensatory mechanisms emerge over time. In this study, we used in vivo genome editing to ablate expression of the Grin1 gene, which encodes the obligate GluN1 subunit of NMDARs, in neurons in the medial PFC of female and male adolescent mice. We assessed synaptic density and function in layer V pyramidal neurons at multiple time points using whole-cell patch-clamp electrophysiology, integrated with confocal imaging of dendritic spine architecture in recorded neurons. NMDAR ablation caused an early decrease in basilar dendritic spine density, followed by a rebound over baseline in spine density and a corresponding increase in AMPAR-mediated synaptic transmission. Inhibitory spontaneous neurotransmission was also increased, suggesting that synaptic compensation maintains an allostatic set point. Our findings demonstrate that NMDAR ablation initially disrupts local PFC networks, followed by recovery via compensatory processes that may be impaired in the disease state.

INTRODUCTION

Schizophrenia is a complex psychiatric illness that affects approximately 0.5% of the global population [1] and can lead to significant reductions in quality and length of life [2]. Abnormal glutamatergic signaling in the prefrontal cortex (PFC) is one of several biomarkers associated with the disease [3] with convergent evidence from genome-wide association studies [4–5], postmortem tissue histology [6–7], and in vivo neuroimaging [8–9] indicating altered expression and function of N-methyl-D-aspartate receptors (NMDARs). Early evidence for the link between glutamatergic signaling and schizophrenia came from studies showing that the administration of NMDAR antagonists such as phencyclidine (PCP) and ketamine induces a psychotomimetic state in healthy individuals [10–11] and worsen symptoms in patients [12–14]. Repeated NMDAR antagonist administration in rodents and primates also leads to cognitive deficits and a progressive decrease in the synchronous firing of PFC neurons, which may be related to a loss of synaptic connectivity [15–19]. This is consistent with human postmortem tissue studies demonstrating a reduction in dendritic spine density in patients with schizophrenia, specifically in the basilar dendrites of deep layer III neurons in the dorsolateral PFC (dlPFC) [20–21]. These deficits in neural synchrony and spine architecture support the theory of activity-dependent disconnection [18, 22–24], which posits that NMDAR loss drives spike timing defects in neurons and leads to subsequent weakening of neural circuits in the PFC [25].

NMDARs are heterotetrameric proteins containing two obligatory GluN1 subunits encoded by the Grin1 gene and two GluN2 and/or GluN3 subunits [26]. Initial research on the impact of NMDAR ablation upon neuroanatomy and physiology was conducted using mice with a homozygous genetic knockout of Grin1, which prevents the assembly of functional NMDARs [27]. However, *Grin1*$^{-/-}$ mice die 8-15 hours after birth due to respiratory failure, making them an unsuitable model for studying the long-term effects of NMDAR hypofunction [28]. The lethal effect of full Grin1 knockout can be avoided by using a more targeted approach; for instance, sparse Grin1 deletion in cultured cells or region-specific knockout in vivo. The impacts of these manipulations differ substantially depending on the brain region, developmental window, and method. Global knockdown of Grin1 to 10% of normal levels leads to reduced dendritic spine density in striatal medium spiny

neurons [29] and unstable spines and reduced spine density in organotypic hippocampal slices [30]. In contrast, spiny stellate cells in layer IV of the barrel cortex have increased spine density in a cortical Grin1 knockout mouse [31].

These structural changes in dendritic spine architecture can also be associated with complex changes in excitatory synaptic transmission. Conditional genetic knockout of Grin1 in cortex and hippocampus with Nex-Cre mice leads to decreased spine density and a shortened lifespan of less than one month, but increased AMPAR-mediated synaptic transmission due to greater presynaptic axon bouton volume and postsynaptic density area [32]. Sparse conditional knockout of Grin1 in cultured hippocampal neurons also increases AMPAR-mediated synaptic transmission, but with no corresponding change in dendritic spine density [33]. This study also indicates that the timing of NMDAR manipulation may dictate functional consequences, as there was no change in AMPAR-mediated synaptic transmission when Grin1 was deleted in the hippocampus of mature mice (>P60). The temporal window for efficacy of NMDAR manipulation may vary between brain regions, as the effects of Grin1 deficiency on excitatory synaptic function in the mouse medial PFC (mPFC) can be rescued by restoring NMDAR expression in adulthood [34], indicating that the mature mPFC retains some of its capacity for neuroplasticity.

Taken together, the prior literature provides evidence that loss of NMDAR function leads to changes in spine density and excitatory synaptic transmission, yet there is a critical lack of knowledge regarding the effects of NMDAR manipulation in the frontal cortex during adolescence. This is a clinically relevant developmental period characterized by significant synaptic pruning [35] and the beginning of symptom onset in schizophrenia [36–40]. We addressed this question using recent advances in genome editing that have made it possible to perform localized and chronic genetic manipulations in the mature nervous system in vivo [41–42]. We utilized clustered regularly interspaced short palindromic repeats (CRISPR)-Cas9 technology to delete the Grin1 gene encoding the obligate GluN1 subunit of NMDARs in mouse mPFC and examined the effects of NMDAR ablation upon the progression of this synaptic reorganization by measuring synaptic strength and density at multiple time points during adolescence and early adulthood. We integrated electrophysiological measurements

with confocal imaging of dendritic spines in order to understand how complex interrelated changes in neurotransmission and synaptic architecture may unfold over time in response to the loss of NMDARs.

MATERIALS & METHODS

Animals

Mice expressing a Cre-dependent Cas9-GFP transgene [43] were maintained on a C57Bl/6J genetic background and housed on a 12-h light cycle (0600–1800 h) at ~23ºC with ad libitum access to food and water. All experimental procedures were conducted between 0800h – 1800h and performed using comparable numbers of female and male mice. All procedures were approved by the Institutional Animal Care and Use Committee at the University of Minnesota and observed the NIH Guidelines for the Care and Use of Laboratory Animals.

Viral vectors

Adeno-associated viral vectors were generated by the Viral Innovation Core at the University of Minnesota. We targeted the Grin1 gene for genome editing using a gRNA sequence [CCGCGCCGATGTTGACAATCT; "gRNA(Grin1)"] expressed using AAV9-U6-gRNA(Grin1)-hSyn-mCherry-Cre (titer: 2.16E13 GC/ml), with a control gRNA targeting LacZ [TGCGAATACGCCCACGCGAT; "gRNA(LacZ")] expressed using AAV9-U6-gRNA(LacZ)-hSyn-mCherry-Cre (titer: 1.75E13 GC/ml) [44]. Both viral vectors expressed gRNA in tandem with an mCherry-Cre fusion protein to visualize transduced cells and catalyze Cre-dependent Cas9 expression for genome editing, under the control of the human synapsin (hSyn) promoter to target all neurons.

Surgical procedures

As previously described [45], mice between 5-6 weeks old were anesthetized with a ketamine/xylazine cocktail (100/10 mg/kg, i.p.), and surgical procedures were performed using a stereotaxic alignment system (Kopf Instruments, Tujunga, CA, USA) with a heating pad to maintain body temperature. Virus was infused

76 bilaterally (500 nL each side at 120 nL/min) into the mPFC (AP: +1.80 mm, ML: ±0.35 mm, DV: −2.2 mm
77 from bregma). After infusion, the needle was left in place for five minutes to allow for viral diffusion, then
78 gradually retracted over the course of approximately two minutes. Mice were administered carprofen (10 mg/kg,
79 s.c.) on the day of surgery and for three subsequent days. Data were collected two weeks (14-27 days), four
80 weeks (28-41 days), or six weeks (42-55 days) post-surgery.
81
82 **Immunohistochemistry for virus expression**
83 Mice were deeply anesthetized using sodium pentobarbital (Fatal-Plus, Vortech Pharmaceuticals) and
84 transcardially perfused with ice cold 0.01 M PBS followed by ice cold 4% PFA in 0.01 M PBS. Brains were
85 extracted and post-fixed in 4% PFA at 4ºC overnight, then transferred to a 10% sucrose solution. Coronal mPFC
86 sections were cut in PBS at 50 microns on a vibratome (Leica VT1000S) and stored at -20ºC in a cryoprotectant
87 solution containing 50 mM phosphate buffer, 876 mM sucrose, and 30% ethylene glycol. Upon use, slices were
88 washed 3 x 15 mins in PBS and incubated with blocking buffer (PBS with 2% normal horse serum (NHS) and
89 1% Triton-X100) for two hours at room temperature, then incubated with primary antibody (chicken polyclonal
90 anti-GFP, Abcam ab13970, 1:2000) for 72 hours at 4ºC. We did not include a primary antibody for mCherry
91 because the endogenous mCherry signal was bright enough to be detected without amplification. Sections were
92 washed 3 x 15 minutes and incubated overnight with secondary antibody (donkey anti-chicken Alexa Fluor 488,
93 Jackson Immuno Research Labs item 703-545-155, 1:300) at 4ºC. Slices were washed once for 15 minutes with
94 PBS, incubated with DAPI nucleic acid stain (Invitrogen, 1:5000) in PBS with 0.03% Triton-X100, 1% bovine
95 serum albumin, 1% normal donkey serum, and 0.01% sodium azide (pH 7.2) for 20 min, and washed three times
96 with PBS for 15 min, 90 min, and 120 min. Slices were mounted in PBS and coverslipped onto glass slides
97 using ProLong Diamond Antifade without DAPI mountant (Thermo Fisher Scientific). Slides were imaged on
98 a Keyence BZX fluorescence microscope under a 10x objective using mCherry and DAPI filter cubes. BZX
99 Analyzer software was used to stitch multi-channel tiled 10x z-stack images into a single image.
100

101 **Brain slice electrophysiology**

102 As previously described [46], mice were deeply anesthetized with isoflurane and perfused with 10 mL
103 ice-cold sucrose cutting solution containing (in mM): 200 sucrose, 1.9 KCl, 1.2 NaH_2PO_4, 33 $NaHCO_3$, 10
104 glucose, 0.4 ascorbic acid, 6 $MgCl_2$, 0.5 $CaCl_2$. Mice were subsequently decapitated and brains were quickly
105 removed then placed in ice-cold sucrose cutting solution. Coronal slices (240 µm thick) containing mPFC were
106 collected using a vibratome (Leica VT1000S) and allowed to recover while submerged in artificial cerebrospinal
107 fluid (aCSF) containing (in mM): 119 NaCl, 2.5 KCl, 1 NaH_2PO_4, 26.2 $NaHCO_3$, 11 glucose, 0.4 ascorbic acid,
108 4 $MgCl_2$, 1 $CaCl_2$. Slices recovered in warm aCSF (33ºC) for 10 min and then equilibrated to room temperature
109 for at least thirty minutes before use. Slices were transferred to a submerged recording chamber and continuously
110 perfused with recording aCSF containing (in mM): 125 NaCl, 2.5 KCl, 25 $NaHCO_3$, 10 glucose, 0.4 ascorbic
111 acid, 1.3 $MgCl_2$, 2 $CaCl_2$ at a rate of 2 mL/min at room temperature. All solutions were continuously oxygenated
112 (95% O_2/5% CO_2).

113 Virally transduced pyramidal neurons in layer V of the mPFC (including anterior cingulate, prelimbic,
114 and infralimbic cortex) were identified by expression of mCherry using an Olympus BX51W1 microscope.
115 Whole-cell voltage-clamp recordings were made with borosilicate glass electrodes (3–4.5 MΩ) filled with (in
116 mM): 120 $CsMeSO_4$, 15 CsCl, 10 TEA-Cl, 8 NaCl, 10 HEPES, 5 EGTA, 5 QX-314, 4 ATP-Mg, 0.3 GTP-Na
117 and 0.13% neurobiotin (pH 7.2-7.3). For AMPAR current-voltage measurements, spermine (0.1 mM) was added
118 to the internal solution, with correction for a liquid junction potential of approximately 8 mV in this experiment
119 only.

120 Excitatory postsynaptic currents (EPSCs) were electrically evoked at 0.33 Hz using a glass monopolar
121 electrode placed in layer V/VI, and pharmacologically isolated using GABA-A receptor antagonist picrotoxin
122 (50 µM, Tocris) and GABA-B receptor antagonist SCH 59011 (10 µM, Tocris). AMPAR-mediated EPSCS
123 were measured at a holding potential of -70 mV. NMDAR-mediated EPSCs were measured 50 ms following
124 stimulation at a holding potential of +40 mV. Inhibitory postsynaptic currents (IPSCs) were measured at +10
125 mV and pharmacologically isolated using the NMDAR antagonist D-APV (50 µM, R&D Systems) and the

126 AMPAR antagonist NBQX (10 μM, R&D Systems). Miniature synaptic currents (mEPSCs and mIPSCs) were
127 measured in the presence of tetrodotoxin (500 nM, Fisher Scientific) to block the generation of action potentials.
128 All recordings were performed using a MultiClamp 700B amplifier (Molecular Devices) and Dendrite
129 digitizer (Sutter Instrument), filtered at 2 kHz, and digitized at 10 kHz. Data acquisition was performed using
130 SutterPatch software version 2.3 in Igor Pro version 8.04 (WaveMetrics). Easy Electrophysiology software
131 version 2.8.0 (RRID:SCR_021190) was used for analysis of synaptic currents. For mEPSCs and mIPSCs, at
132 least 200 events per cell were acquired across 20 second sweeps, filtered at 1.5 kHz and detected using an
133 amplitude threshold of 5 pA and a detection criterion of 4.00 [47].
134
135 **Confocal imaging and analysis of dendritic spines**
136 Following whole-cell patch-clamp recordings with internal pipette solution containing neurobiotin, the
137 pipette was slowly retracted until a gigaohm seal was formed, indicating successful separation from the
138 membrane of the recorded cell that was preserved for morphological analysis. Slices were fixed in 4% PFA for
139 a minimum of 12 hours and washed 3 x 15 minutes with PBS prior to staining. Nonspecific binding was blocked
140 with a solution containing 2% NHS in PBS with 0.05% Tween-20 and 0.2% Triton-X100 for 3 hours at room
141 temperature, followed by 18 hours in Cy5-streptavidin (Cytiva – Amersham) diluted 1:500 in the same blocking
142 solution at 4ºC. Sections were rinsed three times in PBS containing 0.1% Tween-20, mounted from DI H_2O,
143 and coverslipped onto glass slides using ProLong Gold Antifade with DAPI mountant (Thermo Fisher
144 Scientific).
145 Dendritic spines were imaged using a Leica Stellaris 8 confocal microscope operated by a workstation
146 running Leica LAS X acquisition software (version 4.6.1). The laser's excitation wavelength was set to 644 nm
147 to image Cy5-streptavidin while minimizing signal from viral mCherry expression. Cells were imaged first with
148 a 20x oil immersion objective 0.75 NA with an xy pixel size of 568 nm and a z-step size of 0.96 microns to
149 provide an overall view of the dendritic arbor, and then spines were imaged with a 63x oil immersion objective
150 1.4 NA with an xy pixel size of 93 nm and a z-step size of 0.28 microns. Apical dendrites of layer V neurons

151 were imaged in layer I of the mPFC, which is the site of synaptic contacts between layer V and layer II/III mPFC
152 neurons [48]. The layer V neuron's longest basilar dendrite and its branches were also imaged [20,
153 49]. Lightning deconvolution was applied to all 63x images to improve resolution.

154 All spine data was analyzed using Bitplane Imaris software (version 10.1). Images were first masked to
155 remove background signal, and filaments were manually drawn to capture the path of the dendrites. Spines were
156 detected using the seed point classification algorithm and manually corrected to remove duplicate seed points
157 and/or add missing spines as needed. Spine morphology was automatically classified using the built-in Matlab
158 toolbox in Imaris.

159

160 **Statistical analysis**

161 Similar numbers of male and female animals were used in all experiments, with sample sizes indicated
162 in figure legends (n = number of cells, N = number of animals) and illustrated by individual data points in
163 figures, with a visual distinction between cells from females (open circles) and males (filled circles). Sex was
164 included as a variable in factorial ANOVA models analyzed using GraphPad Prism version 10, with repeated
165 measures on within-subject factors. Significant ANOVA interactions were decomposed by analyzing simple
166 effects (i.e., the effect of one variable at each level of the other variable). Significant main effects were analyzed
167 using Fisher's Least Significant Difference (LSD) post-hoc tests. The Type I error rate was set to $\alpha = 0.05$ (two-
168 tailed) for all comparisons. All summary data are displayed as mean +/- SEM. Traces in figures have had
169 stimulus artifacts removed. All figures were created in BioRender.

170

171 **RESULTS**

172 **Validation of NMDAR Ablation using in vivo Genome Editing**

173 To eliminate NMDAR expression, we used transgenic male and female mice expressing Cas9 and eGFP
174 from the Rosa26 locus in a Cre-dependent fashion [43]. To activate Cas9 expression in mPFC neurons, we
175 performed bilateral stereotaxic injection of an adeno-associated virus (AAV), with expression of mCherry-Cre

176 driven by the hSyn promoter sequence. The same AAV vector also expressed a guide RNA targeting the Grin1
177 gene [44], which encodes the obligate GluN1 subunit of NMDARs (Fig 1A). As a control, separate groups of
178 mice were injected with a virus expressing a guide RNA for LacZ (a bacterial gene not present in mammals) in
179 place of the Grin1 guide RNA. Stereotaxic injection of these AAV vectors was performed in adolescent mice at
180 5-6 weeks of age, a time point selected to mirror a developmental period associated with significant pruning of
181 cortical networks [50, 51] and the onset of schizophrenia-related symptoms in some patients [52]. We confirmed
182 viral expression in the mPFC based on mCherry fluorescence, with co-localized GFP fluorescence by individual
183 neurons indicating Cre-mediated transgene expression (Fig 1B).

184 To confirm successful ablation of the Grin1 gene and subsequent loss of NMDAR function in virally
185 transduced cells, we performed whole-cell patch-clamp recordings from layer V pyramidal neurons in acute
186 mPFC brain slices, prepared 2-6 weeks after stereotaxic surgery. NMDAR current was measured by recording
187 electrically-evoked excitatory postsynaptic currents (EPSCs) at +40 mV and calculating the amplitude at 50 ms
188 post-stimulus, by which point the fast AMPAR current has decayed (Fig. 1C) [53]. AMPAR current was
189 measured by recording EPSCs at -70 mV and calculating the peak amplitude. At all timepoints, there was a
190 significant reduction in the NMDAR/AMPAR ratio in the Grin1 group compared to the control group (Fig 1D).
191 The half-width of the dual component EPSC (NMDAR+AMPAR) recorded at +40 mV was similarly reduced
192 at all timepoints (Fig 1E). This indicates that the change in the NMDAR/AMPAR ratio is due to a loss of
193 NMDARs, which have slower kinetics and therefore produce a more sustained excitatory current at +40 mV
194 compared to AMPARs.

195

196 **Dendritic Spine Architecture after NMDAR Ablation**

197 To quantify synaptic density after ablation of NMDAR expression, we filled individual neurons with
198 neurobiotin during whole-cell patch-clamp recordings, and then performed confocal imaging of dendritic
199 architecture in the same pyramidal neurons (Fig 2A). Using Imaris software, spines were also automatically
200 classified into four morphological groups: mushroom spines, which tend to be more stable and associated with

201 greater synaptic strength; and filopodia/dendrites, stubby spines, and long/thin spines, which are more immature
202 and weaker [54].

203 In the basilar dendritic arbor (Fig 2B-C), we observed differences between the Grin1 and control groups
204 that varied across time. At 2 weeks, there is a significant decrease in basilar spines in the Grin1 group (Fig 2D),
205 with a corresponding leftward shift in the cumulative probability distribution (Fig 2E), driven primarily by a
206 loss of thin spines and filopodia (Fig 2H). This same trend was observed to a lesser extent at 4 weeks (Fig 2F),
207 with a significant decrease in the density of mushroom spines (Fig. 2I). At six weeks, this pattern reversed (Fig.
208 2D) and the cumulative probability distribution shifted rightward toward a significant *increase* in the Grin1
209 group compared to LacZ (Fig 2G), a pattern most apparent in the less mature spine categories (Fig. 2J). These
210 morphological changes were specifically observed in the basilar dendritic arbor, as no significant changes in
211 total spine density or specific spine categories were observed at any time point in the apical dendritic arbor of
212 the same cells (Fig. S1).

213

214 **Functional Correlates of Synaptic Strength and Density**

215 To investigate the functional implications of these alterations in synaptic architecture, we recorded
216 miniature excitatory postsynaptic currents (mEPSCs) in the presence of tetrodotoxin (500 nM), providing a
217 measure of spontaneous excitatory neurotransmission (Fig 3A). The mEPSC amplitude, which is a correlate of
218 postsynaptic strength, was not significantly changed at any time point (Fig 3B). However, there was a significant
219 increase in mEPSC frequency at 6 weeks (Fig 3C), with a corresponding leftward shift in the cumulative
220 probability distribution of mEPSC inter-event intervals at 4 and 6 weeks (Fig 3F and 3H), but not at 2 weeks
221 (Fig 3D).

222 We also evaluated potential changes in mEPSC frequency as a function of event size. mEPSC amplitude
223 can be influenced by synaptic location – i.e., events that originate at more distal synapses tend to have a smaller
224 amplitude due to dendritic filtering, whereas events that originate closer to the soma tend to be larger [55]. At

225 all timepoints, the relative difference in mEPSC frequency between Grin1 and control groups was similar,
226 regardless of amplitude (Fig 3E, 3G, 3I).
227
228 **Compensatory Changes in Synaptic Transmission**
229 Taken together, the changes in synaptic structure and function described above point towards an initial
230 loss of dendritic spines in the Grin1 group. This is followed by a recovery of dendritic spine density that returns
231 to and overshoots control density, with a corresponding increase in mEPSC frequency. These changes may
232 emerge as a compensatory response to the ablation of NMDARs, so we next investigated other potential
233 compensatory changes in excitatory or inhibitory synaptic transmission. Following six weeks of virus
234 expression, there was no change in the paired-pulse ratio of evoked EPSCs at interstimulus intervals ranging
235 from 25-400 ms (Fig 4A-B). This indicates that presynaptic glutamate release probability was unaffected by
236 NMDAR ablation, and also suggests the increase in mEPSC frequency at the same time point was related to
237 dendritic spine density and synapse number, rather than a change in the probability of glutamate release.
238 We next examined the possibility that NMDAR ablation and corresponding loss of calcium influx could
239 lead to compensatory changes in AMPAR subunit composition, such as increased contribution of AMPARs
240 lacking the GluA2 subunit [56, 57]. Subunit composition can influence the kinetic properties of AMPAR
241 currents, but there was no change at any time point in the half-width of the isolated AMPAR current recorded
242 at -70 mV as part of the NMDAR/AMPAR ratio measurement (Fig 4C). Calcium-permeable AMPARs lacking
243 a GluA2 subunit are blocked by intracellular polyamines at depolarized membrane potentials, producing a non-
244 linear current-voltage relationship. However, following six weeks of virus expression, there was no difference
245 in the AMPAR current-voltage relationship (Fig 4D-E), and no change in the rectification index comparing
246 current passed at depolarized versus hyperpolarized membrane potentials (Fig. 4F). These data suggest that the
247 subunit composition of AMPARs does not change following NMDAR ablation.
248 Given the increase in dendritic spine density and mEPSC frequency following six weeks of virus
249 expression, we also explored potential adaptations at the level of inhibitory synaptic transmission, by recording

250 miniature inhibitory postsynaptic currents (mIPSCs) at this time point (Fig 5A). Following six weeks of virus
251 expression, we observed a significant increase in average mIPSC amplitude (Fig 5B-C), but no change in mIPSC
252 frequency (Fig 5D-E). These results suggest that following protracted NMDAR ablation, the overall excitatory-
253 inhibitory balance of the mPFC network may be maintained by stabilizing at a new allostatic set point (Fig. 5F-
254 G).
255

256 **DISCUSSION**

257 Our findings reveal significant time-dependent structural and functional reorganization of cortical
258 networks following NMDAR manipulation during adolescence. We observed a change in basilar spine density
259 following NMDAR ablation, with initial spine loss in the Grin1 group at earlier time points shifting towards an
260 increase in spine density at 6 weeks. This effect was primarily driven by thin spines, which are associated with
261 weaker synapses and appear or disappear in response to synaptic activity [58], as well as filopodia, which have
262 a short lifespan and may not form functional synapses due to their lack of postsynaptic density [54]. This is
263 consistent with evidence from human postmortem tissue studies showing a selective loss of smaller spines in
264 the cortex of patients with schizophrenia [59, 60]. We did not observe a change in apical spine density at any
265 time point. This suggests that the local mPFC microcircuitry may be more vulnerable to the effects of NMDAR
266 ablation, since basilar dendrites receive inputs from other nearby neurons, whereas apical dendrites receive more
267 long-range cortical and thalamic signals [61]. This basilar-specific effect is consistent with evidence of
268 decreased synchronous firing between pairs of prefrontal neurons following NMDAR blockade [18], which
269 indicates that disruption of local PFC connections may be a key consequence of NMDAR hypofunction.

270 We were surprised that changes in dendritic spine architecture were observed in the basilar but not the
271 apical dendritic arbor of layer V pyramidal neurons. Studies of postmortem tissue from patients with
272 schizophrenia have documented a reduction in dendritic spine density in the basilar dendrites of deep layer III
273 neurons in the dlPFC. Based on these previous studies, it has been suggested that apical dendrites in layer V
274 neurons may be vulnerable to spine loss in schizophrenia, since deep layer apical dendrites and superficial layer

275 basilar dendrites both receive inputs from the mediodorsal nucleus of the thalamus within layer III [62]. In
276 contrast, the significant increase in basilar spine density that we observed at 6 weeks suggests that the network
277 is overcompensating for early initial spine loss. This may be attributed to the selective nature of our
278 manipulation; while spine density decreased as we predicted at 2 and 4 weeks, neurons were able to adapt by
279 producing more spines because we did not alter synaptic architecture proteins that are implicated in spine loss
280 in schizophrenia, such as Cdc42 and Duo [62]. This would explain why we observed an increase in spine density
281 at later time points, despite our initial prediction that loss of NMDARs would lead to a reduction in synapse
282 density due to activity-dependent disconnection [18]. Our findings indicate that NMDAR ablation alone is not
283 sufficient to induce long-lasting deficits in spine density, and suggests that other risk factors for the disease
284 – whether genetic or environmental – could also play a role in the failure to recover from loss of neuropil
285 observed in patients with schizophrenia.

286 We examined whether the changes in spine density were associated with functional consequences at the
287 synaptic level, and observed a significant increase in mEPSC frequency at 6 weeks. There were no compensatory
288 changes in presynaptic glutamate release or AMPAR subunit composition, indicating that the mEPSC frequency
289 change was primarily driven by the alterations in basilar spine density. Interestingly, we also observed an
290 increase in inhibitory signaling, with mIPSC amplitude significantly greater in the Grin1 group at 6 weeks.
291 While it was surprising that there were no electrophysiological changes observed at 2 weeks given the significant
292 reduction in basilar spine density at that time point, this may be attributed to the fact that early spine loss was
293 primarily due to a reduction in weaker, less stable spines such as thin spines and filopodia, which may have a
294 smaller contribution to detectable levels of synaptic transmission [54]. In contrast, mushroom spine density has
295 a much smaller decrease in Grin1 mice at 2 weeks. At 6 weeks, the density of mushroom spines, which are more
296 stable and associated with stronger synapses [63], is equivalent in the Grin1 and control groups and the density
297 of weaker spines is significantly greater, which may be sufficient to produce the observed increase in mEPSC
298 frequency. Overall, these results suggest that subtle changes in synaptic architecture may precede functional

consequences for the network, with initial loss of immature spines leading to a compensatory increase in connectivity and neurotransmission at later time points.

While our study is focused on the effects of pan-neuronal NMDAR ablation, the question of whether pyramidal neurons or interneurons are primarily affected by NMDAR hypofunction is a key question in the field, with the goal of developing precisely targeted treatments. Abnormal glutamatergic postsynaptic proteins and excessive synaptic pruning in excitatory neurons [64–67] may lead to a subsequent downregulation of feedback inhibition, as reflected by decreased interneuron expression of the activity-dependent proteins glutamate decarboxylase 67 and parvalbumin [64, 68, 69]. However, interneurons may be the initial locus of dysfunction: patients with schizophrenia have lower GABA synthesis [70], and reduced expression of interneuron neuropeptides and GABA-A receptor subunits [71]. In addition, reduced GAD67 expression is sufficient to induce schizophrenia-related behavioral phenotypes and altered excitatory and inhibitory synaptic transmission [72, 73]. Interneurons are also preferentially targeted by NMDAR antagonists due to their more depolarized membrane potential [74], raising the question of whether previous studies using NMDAR antagonism as a model for schizophrenia have exerted greater effects upon inhibitory neurons than excitatory neurons. While several genetic manipulations have been developed to target Grin1 in interneurons [75–79], there is rarely a direct comparison with excitatory neurons following NMDAR manipulation, thus limiting our ability to draw conclusions about the relative contributions of each neuronal population to the observed phenotypes. Although we did not directly assess the effects of targeted NMDAR ablation in pyramidal cells versus interneurons, one potential explanation for the increased excitatory signaling that we observed at 6 weeks following early spine loss would be that altered inhibitory neurotransmission may initially weaken excitatory activity, until pyramidal neurons are able to compensate for increased inhibition at later time points by upregulating excitatory activity and producing more dendritic spines.

Our data address questions regarding the emergence of compensatory synaptic mechanisms, which are central to developing our understanding of schizophrenia. Symptom onset may be triggered in patients by the interaction of multiple layered risk factors [80]. One theory of the disease is that genetic mutations affecting

synapse formation and maintenance cause latent defects in cortical connectivity that are masked by the hyperconnected state of the brain in early development, but as extraneous synapses are pruned during adolescence, these vulnerabilities are laid bare and symptoms begin to occur in patients [39]. In our model, the cellular mechanisms of spine formation and maintenance were unchanged, and therefore early synaptic defects could be compensated for by the production of additional immature spines. Studying the effects of an isolated Grin1 manipulation may help us understand why first-degree relatives of patients who have Grin1 mutations but no additional genetic risk factors do not develop schizophrenia, or why patients with fewer biological or environmental risk factors are able to successfully recover from first-episode psychosis. In contrast, other patients may have altered gene expression related to neuronal survival [81] and architecture, such as complement-mediated synaptic pruning [66, 82], thus limiting the brain's ability to adapt to insults and leading to more severe or long-lasting symptoms. Further study will be needed to examine how synaptic changes such as NMDAR ablation interact with other risk factors to influence processes of synaptic dysfunction and compensation relevant to schizophrenia. However, the preclinical success of newly developed therapies to treat NMDAR hypofunction is an encouraging sign that these synaptic deficits and associated cognitive symptoms may be able to be treated in patients [83].

ACKNOWLEDGEMENTS

Viral vectors used in this study were generated by the University of Minnesota Viral Innovation Core and the Center for Neural Circuits in Addiction (P30 DA048742). We thank the University of Minnesota University Imaging Core (SCR_020997) for the use of their facilities to conduct confocal imaging and analysis of dendritic spines, and Dr. Matthew Hearing for advice regarding electrophysiology experiments.

AUTHOR CONTRIBUTIONS

RMD, NMG, and PER were responsible for study design. RMD conducted and analyzed electrophysiology recordings and performed immunohistochemistry protocols. RMD and HA performed intracranial injections of viral vectors generated by EMFV. RMD, LBC, ATP, HA, and JSM conducted confocal imaging and analysis of dendritic spines. RMD and PER wrote the original draft of the manuscript, which all authors reviewed and edited before submission.

FUNDING

This work was supported by grants from the National Institutes of Health (T32MH115886 and F31MH133285 to RMD; P50MH119569 to NMG and PER); the University of Minnesota's MnDRIVE (Minnesota's Discovery, Research, and Innovation Economy) initiative (PER); the University of Minnesota Life Sciences Summer Undergraduate Research Program (ATP); and the University of Minnesota Undergraduate Career Opportunities in Neuroscience and Undergraduate Research Opportunities Program (HA).

COMPETING INTERESTS

The authors declare no competing interests.

DATA AVAILABILITY STATEMENT

Data are available from the corresponding author upon request.

REFERENCES

1. Saha S, Chant D, Welham J, McGrath J. A systematic review of the prevalence of schizophrenia. PLoS Med. 2005;2:0413–0433.

2. Hjorthøj C, Stürup AE, McGrath JJ, Nordentoft M. Years of potential life lost and life expectancy in schizophrenia: a systematic review and meta-analysis. The Lancet Psychiatry. 2017;4:295–301.

3. Moghaddam B, Javitt D. From revolution to evolution: The glutamate hypothesis of schizophrenia and its implication for treatment. Neuropsychopharmacology. 2012;37:4–15.

4. Timms AE, Dorschner MO, Wechsler J, Choi KY, Kirkwood R, Girirajan S, et al. Support for the N - Methyl-D-Aspartate Receptor Hypofunction Hypothesis of Schizophrenia From Exome Sequencing in Multiplex Families. JAMA Psychiatry. 2013;70:582–590.

5. Ohi K, Hashimoto R, Ikeda M, Yamamori H, Yasuda Y, Fujimoto M, et al. Glutamate Networks Implicate Cognitive Impairments in Schizophrenia: Genome-Wide Association Studies of 52 Cognitive Phenotypes. Schizophr Bull. 2015;41:909–918.

6. Beneyto M, Meador-Woodruff JH. Lamina-specific abnormalities of NMDA receptor-associated postsynaptic protein transcripts in the prefrontal cortex in schizophrenia and bipolar disorder. Neuropsychopharmacology. 2008;33:2175–2186.

7. Catts VS, Lai YL, Weickert CS, Weickert TW, Catts S V. A quantitative review of the postmortem evidence for decreased cortical N-methyl-d-aspartate receptor expression levels in schizophrenia: How can we link molecular abnormalities to mismatch negativity deficits? Biol Psychol. 2016;116:57–67.

8. Poels EMP, Kegeles LS, Kantrowitz JT, Slifstein M, Javitt DC, Lieberman JA, et al. Imaging glutamate in schizophrenia: Review of findings and implications for drug discovery. Mol Psychiatry. 2014;19:20–29.

9. Bustillo JR, Upston J, Mayer EG, Jones T, Maudsley AA, Gasparovic C, et al. Glutamatergic hypo-function in the left superior and middle temporal gyri in early schizophrenia: a data-driven three-dimensional proton spectroscopic imaging study. Neuropsychopharmacology. 2020;45:1851–1859.

10. Javitt DC, Zukin RS. Recent advances in the phencyclidine model of schizophrenia. Am J Psychiatry. 1991;148:1301–1308.

11. Umbricht D, Schmid L, Koller R, Vollenweider FX, Hell D, Javitt DC. Ketamine-Induced Deficits in Auditory and Visual Context-Dependent Processing in Healthy Volunteers: Implications for Models of Cognitive Deficits in Schizophrenia. Arch Gen Psychiatry. 2000;57:1139–1147.

12. Lahti AC, Koffel B, Laporte D, Tamminga CA. Subanesthetic doses of ketamine stimulate psychosis in schizophrenia. Neuropsychopharmacology. 1995;13:9–19.

13. Malhotra AK, Pinals DA, Adler CM, Elman I, Clifton A, Pickar D, et al. Ketamine-induced exacerbation of psychotic symptoms and cognitive impairment in neuroleptic-free schizophrenics. Neuropsychopharmacology. 1997;17:141–150.

14. Lahti AC, Weiler MA, Michaelidis T, Parwani A, Tamminga CA. Effects of ketamine in normal and schizophrenic volunteers. Neuropsychopharmacology. 2001;25:455–467.

15. Jentsch JD, Tran A, Le D, Youngren KD, Roth RH. Reduces Mesoprefrontal Dopamine Utilization and Impairs Prefrontal Cortical-Dependent Cognition in the Rat. 1997;17:92–99.

16. Wang M, Yang Y, Wang C-J, Gamo NJ, Jin LE, Mazer JA, et al. NMDA receptors subserve persistent neuronal firing during working memory in dorsolateral prefrontal cortex. Neuron. 2013;77:736–749.

17. Blackman RK, Macdonald AW 3rd, Chafee M V. Effects of ketamine on context-processing performance in monkeys: a new animal model of cognitive deficits in schizophrenia. Neuropsychopharmacol Off Publ Am Coll Neuropsychopharmacol. 2013;38:2090–2100.

18. Zick JL, Blackman RK, Crowe DA, Amirikian B, DeNicola AL, Netoff TI, et al. Blocking NMDAR Disrupts Spike Timing and Decouples Monkey Prefrontal Circuits: Implications for Activity-Dependent Disconnection in Schizophrenia. Neuron. 2018;98:1243-1255.e5.

19. Vinnakota C, Hudson MR, Ikeda K, Ide S, Mishina M, Sundram S, et al. Effects of NMDA receptor antagonists on working memory and gamma oscillations, and the mediating role of the GluN2D subunit. Neuropsychopharmacology. 2025:1–11.

20. Glantz LA, Lewis DA. Decreased dendritic spine density on prefrontal cortical pyramidal neurons in schizophrenia. Arch Gen Psychiatry. 2000;57:65–73.

21. Lewis DA, González-Burgos G. Neuroplasticity of neocortical circuits in schizophrenia. Neuropsychopharmacology. 2008;33:141–165.

22. Friston KJ. The disconnection hypothesis. Schizophr Res. 1998;30:115–125.

23. Stephan KE, Friston KJ, Frith CD. Dysconnection in schizophrenia: from abnormal synaptic plasticity to failures of self-monitoring. Schizophr Bull. 2009;35:509–527.

24. Zick JL, Crowe DA, Blackman RK, Schultz K, Bergstrand DW, DeNicola AL, et al. Disparate insults relevant to schizophrenia converge on impaired spike synchrony and weaker synaptic interactions in prefrontal local circuits. Curr Biol. 2022;32:14-25.e4.

25. Eryilmaz H, Tanner AS, Ho NF, Nitenson AZ, Silverstein NJ, Petruzzi LJ, et al. Disrupted Working Memory Circuitry in Schizophrenia: Disentangling fMRI Markers of Core Pathology vs Other Aspects of Impaired Performance. Neuropsychopharmacology. 2016;41:2411–2420.

26. Hansen KB, Wollmuth LP, Bowie D, Furukawa H, Menniti FS, Sobolevsky AI, et al. Structure, Function, and Pharmacology of Glutamate Receptor Ion Channels. Pharmacol Rev. 2021;73:298–487.

27. Schüler T, Mesic I, Madry C, Bartholomäus I, Laube B. Formation of NR1/NR2 and NR1/NR3 heterodimers constitutes the initial step in N-methyl-D-aspartate receptor assembly. J Biol Chem. 2008;283:37–46.

28. Forrest D, Yuzaki M, Soares HD, Ng L, Luk DC, Sheng M, et al. Targeted disruption of NMDA receptor 1 gene abolishes NMDA response and results in neonatal death. Neuron. 1994;13:325–338.

29. Ramsey AJ, Milenkovic M, Oliveira AF, Escobedo-Lozoya Y, Seshadri S, Salahpour A, et al. Impaired NMDA receptor transmission alters striatal synapses and DISC1 protein in an age-dependent manner. Proc Natl Acad Sci U S A. 2011;108:5795–5800.

30. Alvarez VA, Ridenour DA, Sabatini BL. Distinct Structural and Ionotropic Roles of NMDA Receptors in Controlling Spine and Synapse Stability. J Neurosci. 2007;27:7365 LP – 7376.

31. Datwani A, Iwasato T, Itohara S, Erzurumlu RS. NMDA receptor-dependent pattern transfer from afferents to postsynaptic cells and dendritic differentiation in the barrel cortex. Mol Cell Neurosci. 2002;21:477–492.

32. Ultanir SK, Kim JE, Hall BJ, Deerinck T, Ellisman M, Ghosh A. Regulation of spine morphology and spine density by NMDA receptor signaling in vivo. Proc Natl Acad Sci U S A. 2007;104:19553–19558.

33. Adesnik H, Li G, During MJ, Pleasure SJ, Nicoll RA. NMDA receptors inhibit synapse unsilencing during brain development. Proc Natl Acad Sci. 2008;105:5597–5602.

34. Venkatesan S, Binko MA, Mielnik CA, Ramsey AJ, Lambe EK. Deficits in integrative NMDA receptors caused by Grin1 disruption can be rescued in adulthood. Neuropsychopharmacology. 2023;48:1742–1751.

35. Selemon LD. A role for synaptic plasticity in the adolescent development of executive function. Transl Psychiatry. 2013;3:e238–e238.

36. Feinberg I. Schizophrenia: caused by a fault in programmed synaptic elimination during adolescence? J Psychiatr Res;17:319–334.

37. Weinberger DR. Implications of Normal Brain Development for the Pathogenesis of Schizophrenia. Arch Gen Psychiatry. 1987;44:660–669.

38. Lewis DA. Development of the Prefrontal Cortex during Adolescence: Insights into Vulnerable Neural Circuits in Schizophrenia. Neuropsychopharmacology. 1997;16:385–398.

39. Chafee M V, Averbeck BB. Unmasking Schizophrenia: Synaptic Pruning in Adolescence Reveals a Latent Physiological Vulnerability in Prefrontal Recurrent Networks. Biol Psychiatry. 2022;92:436–439.

40. Goodpaster CM, Christensen CR, Alturki MB, DeNardo LA. Prefrontal cortex development and its implications in mental illness. Neuropsychopharmacology. 2025:1–15.

41. Straub C, Granger AJ, Saulnier JL, Sabatini BL. CRISPR/Cas9-Mediated Gene Knock-Down in Post-Mitotic Neurons. PLoS One. 2014;9:e105584.

42. Incontro S, Asensio CS, Edwards RH, Nicoll RA. Efficient, complete deletion of synaptic proteins using CRISPR. Neuron. 2014;83:1051–1057.

43. Platt RJ, Chen S, Zhou Y, Yim MJ, Swiech L, Kempton HR, et al. CRISPR-Cas9 knockin mice for genome editing and cancer modeling. Cell. 2014;159:440–455.

44. Hunker AC, Soden ME, Krayushkina D, Heymann G, Awatramani R, Zweifel LS. Conditional Single Vector CRISPR/SaCas9 Viruses for Efficient Mutagenesis in the Adult Mouse Nervous System. Cell Rep. 2020;30:4303-4316.e6.

45. Brandner DD, Retzlaff CL, Kocharian A, Stieve BJ, Mashal MA, Mermelstein PG, et al. Neuroligin-3 in dopaminergic circuits promotes behavioural and neurobiological adaptations to chronic morphine exposure. Addict Biol. 2023;28:e13247.

46. Anderson EM, Demis S, Wrucke B, Engelhardt A, Hearing MC. Infralimbic cortex pyramidal neuron GIRK signaling contributes to regulation of cognitive flexibility but not affect-related behavior in male mice. Physiol Behav. 2021;242:113597.

47. Clements JD, Bekkers JM. Detection of spontaneous synaptic events with an optimally scaled template. Biophys J. 1997;73:220–229.

48. Reyes A, Sakmann B. Developmental switch in the short-term modification of unitary EPSPs evoked in layer 2/3 and layer 5 pyramidal neurons of rat neocortex. J Neurosci Off J Soc Neurosci. 1999;19:3827–3835.

49. Kolluri N, Sun Z, Sampson AR, Lewis DA. Lamina-Specific Reductions in Dendritic Spine Density in the Prefrontal Cortex of Subjects With Schizophrenia. Am J Psychiatry. 2005;162:1200–1202.

50. Huttenlocher PR. Synaptic density in human frontal cortex — Developmental changes and effects of aging. Brain Res. 1979;163:195–205.

51. Huttenlocher PR, Dabholkar AS. Regional differences in synaptogenesis in human cerebral cortex. J

Comp Neurol. 1997;387:167–178.

53. Rothwell PE, Hayton SJ, Sun GL, Fuccillo M V., Kook Lim B, Malenka RC. Input- and Output-Specific Regulation of Serial Order Performance by Corticostriatal Circuits. Neuron. 2015;88:345–356.

54. Arellano JI, Benavides-Piccione R, Defelipe J, Yuste R. Ultrastructure of dendritic spines: correlation between synaptic and spine morphologies. Front Neurosci. 2007;1:131–143.

55. Williams SR, Stuart GJ. Dependence of EPSP efficacy on synapse location in neocortical pyramidal neurons. Science. 2002;295:1907–1910.

56. Hume RI, Dingledine R, Heinemann SF. Identification of a site in glutamate receptor subunits that controls calcium permeability. Science. 1991;253:1028–1031.

57. Liu SQ, Cull-Candy SG. Synaptic activity at calcium-permeable AMPA receptors induces a switch in receptor subtype. Nature. 2000;405:454–458.

58. Bourne J, Harris KM. Do thin spines learn to be mushroom spines that remember? Curr Opin Neurobiol. 2007;17:381–386.

59. MacDonald ML, Alhassan J, Newman JT, Richard M, Gu H, Kelly RM, et al. Selective Loss of Smaller Spines in Schizophrenia. Am J Psychiatry. 2017;174:586–594.

60. McKinney BC, MacDonald ML, Newman JT, Shelton MA, DeGiosio RA, Kelly RM, et al. Density of small dendritic spines and microtubule-associated-protein-2 immunoreactivity in the primary auditory cortex of subjects with schizophrenia. Neuropsychopharmacol Off Publ Am Coll Neuropsychopharmacol. 2019;44:1055–1061.

61. Spruston N. Pyramidal neurons: Dendritic structure and synaptic integration. Nat Rev Neurosci. 2008;9:206–221.

62. Hill JJ, Hashimoto T, Lewis DA. Molecular mechanisms contributing to dendritic spine alterations in the prefrontal cortex of subjects with schizophrenia. Mol Psychiatry. 2006;11:557–566.

63. Matsuzaki M, Ellis-Davies GCR, Nemoto T, Miyashita Y, Iino M, Kasai H. Dendritic spine geometry is critical for AMPA receptor expression in hippocampal CA1 pyramidal neurons. Nat Neurosci. 2001;4:1086–1092.

64. Lewis DA, Curley AA, Glausier JR, Volk DW. Cortical parvalbumin interneurons and cognitive dysfunction in schizophrenia. Trends Neurosci. 2012;35:57–67.

65. Fromer M, Pocklington AJ, Kavanagh DH, Williams HJ, Dwyer S, Gormley P, et al. De novo mutations in schizophrenia implicate synaptic networks. Nature. 2014;506:179–184.

66. Sekar A, Bialas AR, de Rivera H, Davis A, Hammond TR, Kamitaki N, et al. Schizophrenia risk from complex variation of complement component 4. Nature. 2016;530:177–183.

67. Consortium SWG of the PG. Biological insights from 108 schizophrenia-associated genetic loci. Nature. 2014;511:421–427.

68. Hashimoto T, Volk DW, Eggan SM, Mirnics K, Pierri JN, Sun Z, et al. Gene expression deficits in a subclass of GABA neurons in the prefrontal cortex of subjects with schizophrenia. J Neurosci Off J

Soc Neurosci. 2003;23:6315–6326.

69. Enwright JF, Sanapala S, Foglio A, Berry R, Fish KN, Lewis DA. Reduced Labeling of Parvalbumin Neurons and Perineuronal Nets in the Dorsolateral Prefrontal Cortex of Subjects with Schizophrenia. Neuropsychopharmacology. 2016;41:2206–2214.

70. Ohnuma T, Augood SJ, Arai H, McKenna PJ, Emson PC. Measurement of GABAergic parameters in the prefrontal cortex in schizophrenia: focus on GABA content, GABAA receptor α-1 subunit messenger RNA and human GABA transporter-1 (hGAT-1) messenger RNA expression. Neuroscience. 1999;93:441–448.

71. Hashimoto T, Arion D, Unger T, Maldonado-Avilés JG, Morris HM, Volk DW, et al. Alterations in GABA-related transcriptome in the dorsolateral prefrontal cortex of subjects with schizophrenia. Mol Psychiatry. 2008;13:147–161.

72. Fujihara K, Miwa H, Kakizaki T, Kaneko R, Mikuni M, Tanahira C, et al. Glutamate Decarboxylase 67 Deficiency in a Subset of GABAergic Neurons Induces Schizophrenia-Related Phenotypes. Neuropsychopharmacology. 2015;40:2475–2486.

73. Kolata SM, Nakao K, Jeevakumar V, Farmer-Alroth EL, Fujita Y, Bartley AF, et al. Neuropsychiatric Phenotypes Produced by GABA Reduction in Mouse Cortex and Hippocampus. Neuropsychopharmacology. 2018;43:1445–1456.

74. McCutcheon RA, Krystal JH, Howes OD. Dopamine and glutamate in schizophrenia: biology, symptoms and treatment. World Psychiatry. 2020;19:15–33.

75. Belforte JE, Zsiros V, Sklar ER, Jiang Z, Yu G, Li Y, et al. Postnatal NMDA receptor ablation in corticolimbic interneurons confers schizophrenia-like phenotypes. Nat Neurosci. 2010;13:76–83.

76. Korotkova T, Fuchs EC, Ponomarenko A, von Engelhardt J, Monyer H. NMDA receptor ablation on parvalbumin-positive interneurons impairs hippocampal synchrony, spatial representations, and working memory. Neuron. 2010;68:557–569.

77. Billingslea EN, Tatard-Leitman VM, Anguiano J, Jutzeler CR, Suh J, Saunders JA, et al. Parvalbumin Cell Ablation of NMDA-R1 Causes Increased Resting Network Excitability with Associated Social and Self-Care Deficits. Neuropsychopharmacology. 2014;39:1603–1613.

78. Jadi MP, Behrens MM, Sejnowski TJ. Abnormal Gamma Oscillations in N-Methyl-D-Aspartate Receptor Hypofunction Models of Schizophrenia. Biol Psychiatry. 2016;79:716–726.

79. Uehara JM, Gomez Acosta M, Bello EP, Belforte JE. Early postnatal NMDA receptor ablation in cortical interneurons impairs affective state discrimination and social functioning. Neuropsychopharmacology. 2025;50:1119–1129.

80. Vinogradov S, Chafee M V, Lee E, Morishita H. Psychosis spectrum illnesses as disorders of prefrontal critical period plasticity. Neuropsychopharmacol Off Publ Am Coll Neuropsychopharmacol. 2023;48:168–185.

81. Pandya CD, Kutiyanawalla A, Pillai A. BDNF-TrkB signaling and neuroprotection in schizophrenia. Asian J Psychiatr. 2013;6:22–28.

82. Gallego JA, Blanco EA, Morell C, Lencz T, Malhotra AK. Complement component C4 levels in the cerebrospinal fluid and plasma of patients with schizophrenia. Neuropsychopharmacology. 2021;46:1140–1144.

83. Oosterlaken M, Rogliardo A, Lipina T, Lafon P-A, Tsitokana ME, Keck M, et al. Nanobody therapy rescues behavioural deficits of NMDA receptor hypofunction. Nature. 2025. 2025. https://doi.org/10.1038/s41586-025-09265-8.

FIGURES and FIGURE LEGENDS

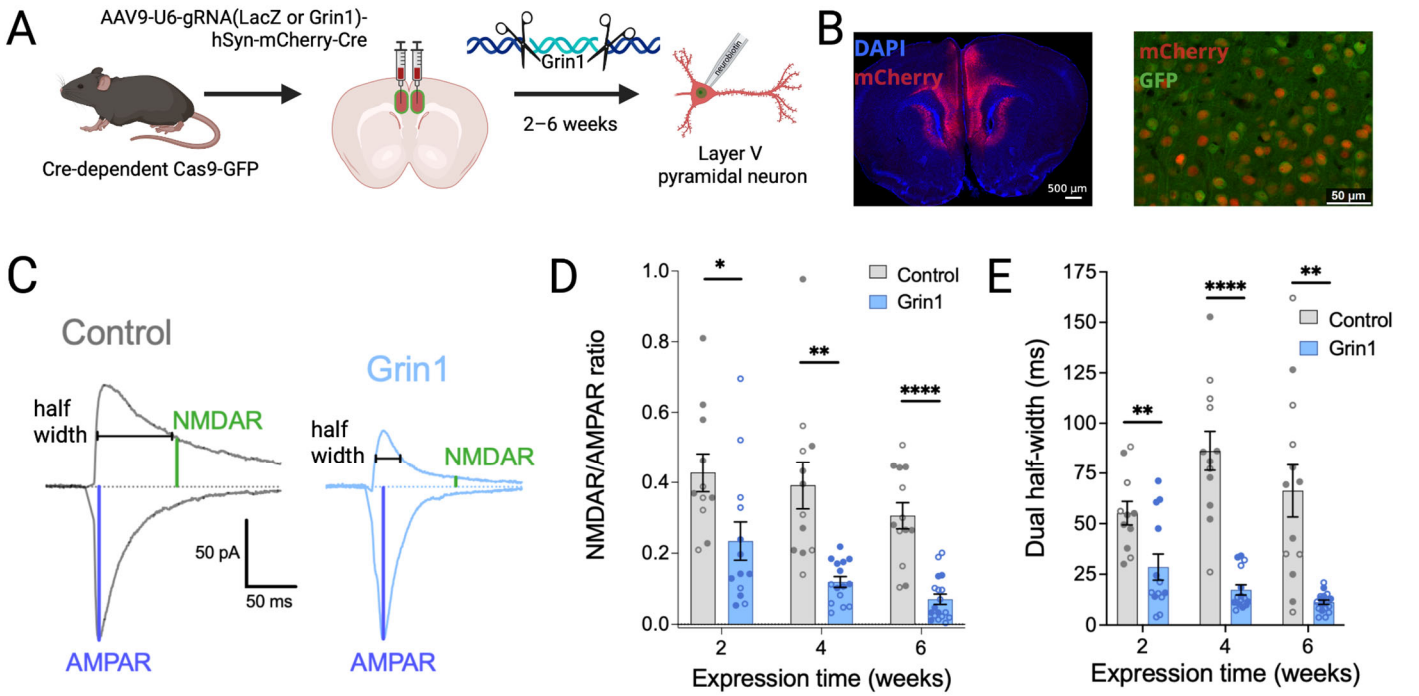

Figure 1. Grin1 ablation decreases NMDAR function. (A) Experimental overview showing mPFC intracranial injection of gRNA virus to ablate Grin1 gene expression, followed by whole-cell patch-clamp recording and neurobiotin cell filling. **(B)** mPFC expression of mCherry and GFP in virally transduced cells (left: 10x magnification tiled image, right: 20x magnification). **(C)** Sample traces of evoked excitatory postsynaptic currents (EPSCs) at -70 mV and +40 mV to measure AMPAR and NMDAR currents, respectively. **(D)** Grin1 ablation reduces NMDAR/AMPAR ratio with a significant main effect of virus ($F_{1,70} = 58.80$, $P < 0.0001$) (control n/N=11/4, 12/5, and 13/6 at 2, 4 and 6 weeks; Grin1 n/N=13/4, 15/6, and 18/6 at 2, 4 and 6 weeks) and **(E)** half-width of the dual component EPSC with a significant main effect of virus ($F_{1,70} = 74.74$, $P < 0.0001$) and time x virus interaction ($F_{2,70} = 3.670$, $P = 0.0305$) (same sample sizes as D). Data are mean ± s.e.m. for all panels; open and closed circles indicate recordings from female and male mice, respectively. *P < 0.05, **P < 0.01, ****P < 0.0001; three-way ANOVA followed by simple effect test; see Data S1 for complete statistics. https://BioRender.com/8iil7j5

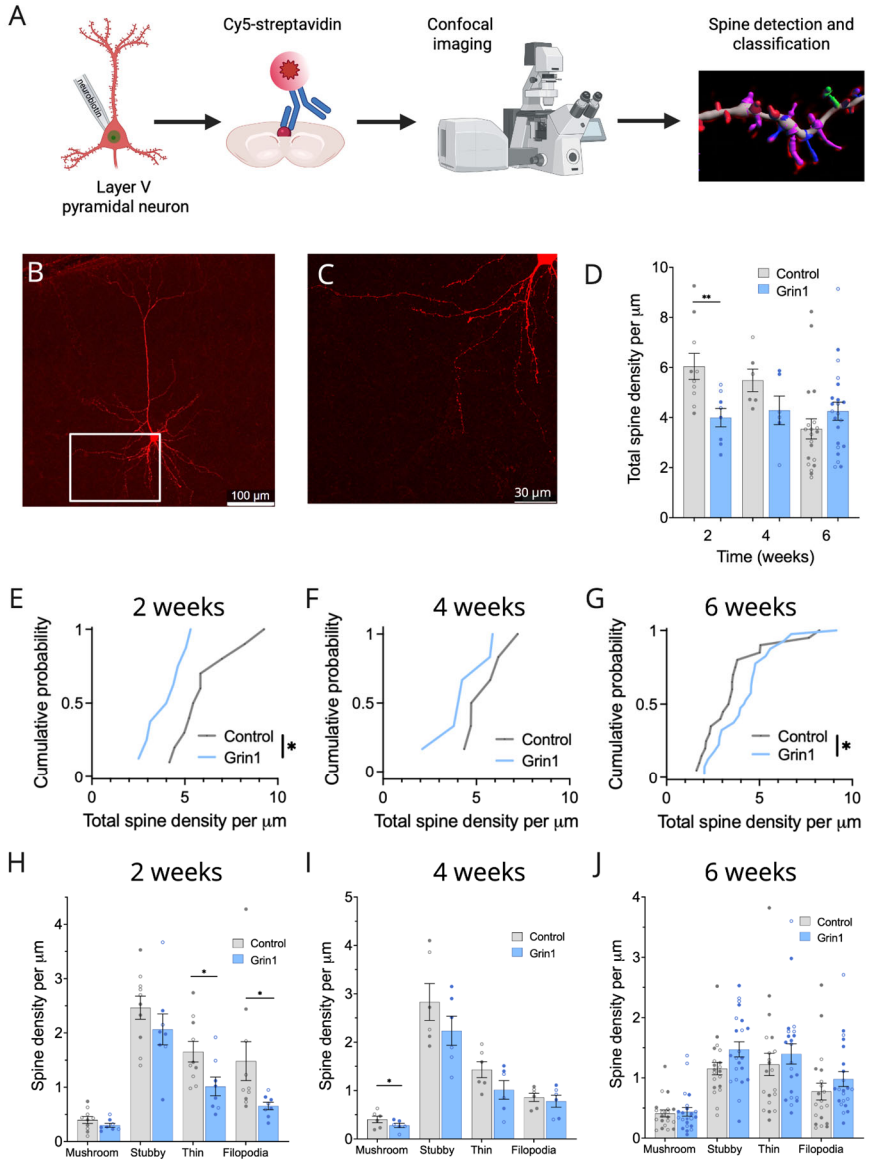

Figure 2. NMDAR ablation causes an initial decrease and subsequent increase in basilar spine density. (A) Schematic showing neurobiotin filling, imaging, and analysis of dendritic spines. **(B-C)** Sample image of the basilar dendrites of a layer V mPFC pyramidal neuron at 20x magnification (B) and 63x magnification (C). **(D)** Decrease in total basilar spine density in the Grin1 group at two weeks, with a trend towards increased density at six weeks (main effect of virus, $F_{1,60}$ = 4.709, P = 0.0340; virus x time interaction, $F_{2,60}$ = 5.307, P = 0.0075) (control n/N = 10/5, 6/4, and 20/12 at 2, 4 and 6 weeks; Grin1 n/N = 8/4, 6/4, and 22/8 at 2, 4 and 6 weeks). **(E, H)** Basilar spine density distribution is significantly reduced in the Grin1 group at two weeks (D = 0.6000, P = 0.0499), driven by significant reductions in thin spines ($F_{1,14}$ = 5.971, P = 0.0284) and filopodia ($F_{1,14}$ = 4.935, P = 0.0433). **(F, I)** Density of mushroom spines is significantly reduced at four weeks ($F_{1,8}$ = 6.689, P = 0.0323). **(G, J)** Basilar spine density distribution is significantly increased at six weeks (D = 0.4364, P = 0.0370), with a trend towards increased density in immature spine categories. Sample sizes for panels E-J are the same as panel D. Data are mean ± s.e.m. for all panels; open and closed circles indicate recordings from female and male mice, respectively. *P < 0.05, **P < 0.01; three-way ANOVA followed by simple effect test (D); Kolmogorov-Smirnov test (E-G); or two-way ANOVA (H-J); see Data S1 for complete statistics. https://BioRender.com/46hxi18

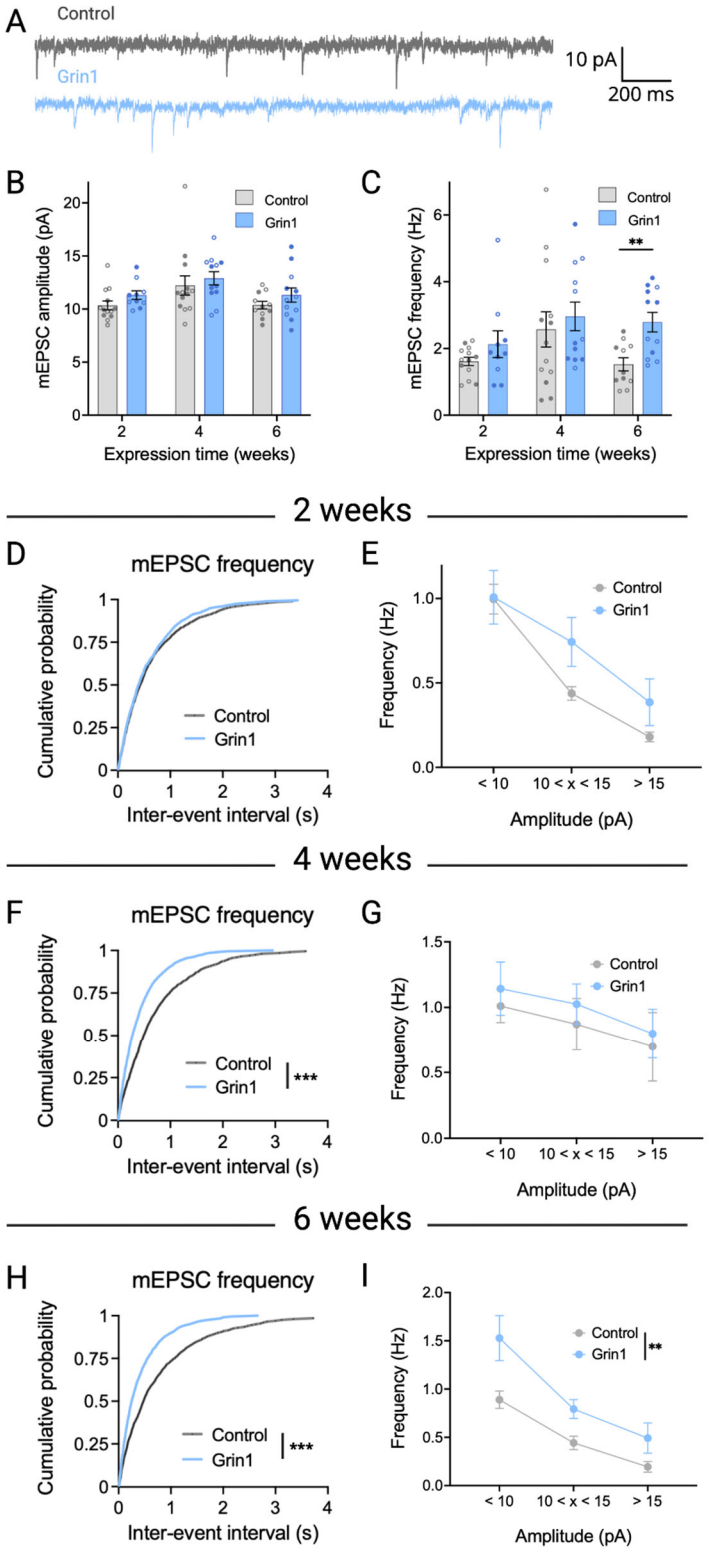

Figure 3. AMPAR-mediated synaptic transmission increases over time following NMDAR ablation. (A) Sample traces of miniature excitatory postsynaptic currents (mEPSCs) at 6 weeks. **(B)** No change in mEPSC amplitude at any time point (control n/N = 13/5, 13/6, and 11/5 at 2, 4 and 6 weeks; Grin1 n/N = 10/4, 12/4, and 12/6 at 2, 4 and 6 weeks). **(C)** mEPSC frequency is significantly increased at six weeks (main effect of virus: $F_{1,59} = 6.063$, $P = 0.0167$). **(D-E)** No change in the distribution of mEPSC frequency across all event sizes at two weeks. **(F)** There is a significant leftward shift in the distribution of mEPSC inter-event interval in the Grin1 group at four weeks ($D = 0.2100$, $P = 0.0003$) and **(H)** six weeks ($D = 0.2150$, $P = 0.0002$), with a similar effect across event amplitudes (main effect of virus at six weeks, $F_{1,21} = 12.12$, $P = 0.0022$) **(G, I).** Sample sizes for panels C-I are the same as panel B. Data are mean ± s.e.m. for all panels; open and closed circles indicate recordings from female and male mice, respectively. $^{**}P < 0.01$, $^{***}P < 0.001$; three-way ANOVA followed by simple effect test (B-C); Kolmogorov-Smirnov test (D, F, H); or two-way ANOVA (E, G, I); see Data S1 for complete statistics. https://BioRender.com/iazf88r

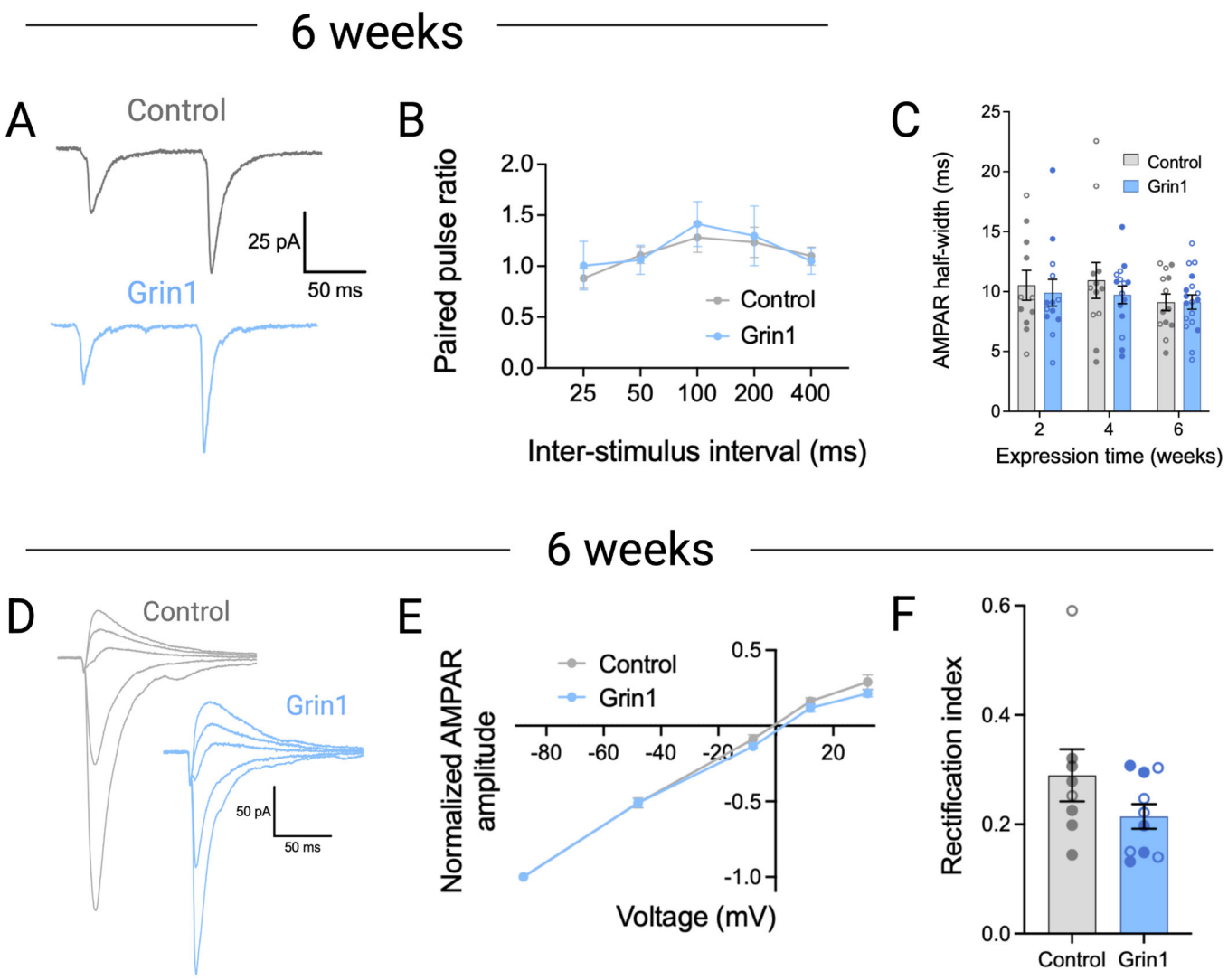

Figure 4. Paired-pulse ratio and AMPAR input-output properties are unchanged after NMDAR ablation. **(A)** Sample traces of EPSCs evoked in response to paired pulse stimulation after 6 weeks of virus expression. **(B)** No significant difference in paired pulse ratio (control n/N = 13-15/7; Grin1 n/N = 11-14/8). **(C)** Half width of the AMPA EPSC is unchanged at all time points (control n/N = 11/4, 12/5, and 13/6 at 2, 4 and 6 weeks; Grin1 n/N = 13/4, 15/6, and 18/6 at 2, 4 and 6 weeks). **(D)** Sample traces of AMPAR EPSCs evoked at different voltages. **(E)** AMPA current-voltage plot shows no significant difference between groups (control n/N = 6-12/7; Grin1 n/N = 3-13/7). **(F)** The rectification index is not significantly different between groups (control n/N = 8/4; Grin1 n/N = 10/7). Data are mean ± s.e.m. for all panels; open and closed circles indicate recordings from female and male mice, respectively. Mixed-effects analysis (B, E); three-way ANOVA (C); or Welch's two-tailed t test (F); see Data S1 for complete statistics. https://BioRender.com/mlt9v8e

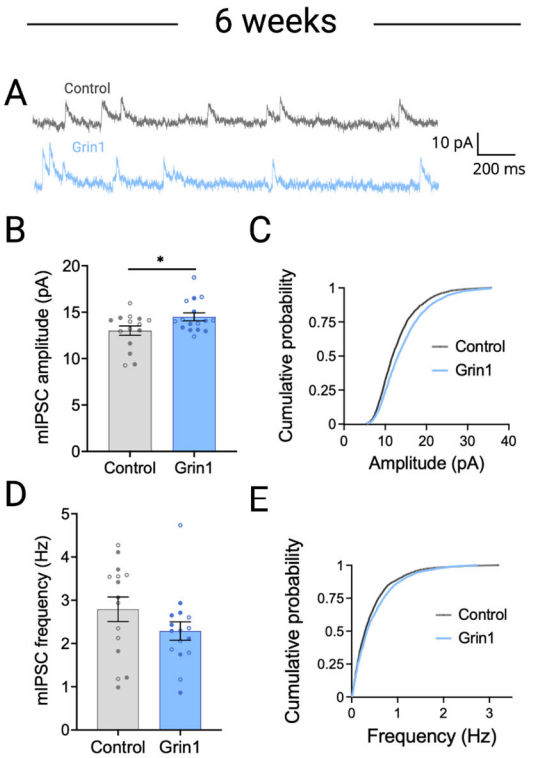

F

Experimental measure	2 weeks	4 weeks	6 weeks
NMDAR/AMPAR ratio	↓	↓	↓
Basilar spine density	↓	↓	↑
mEPSC frequency	–	–	↑
mIPSC amplitude			↑

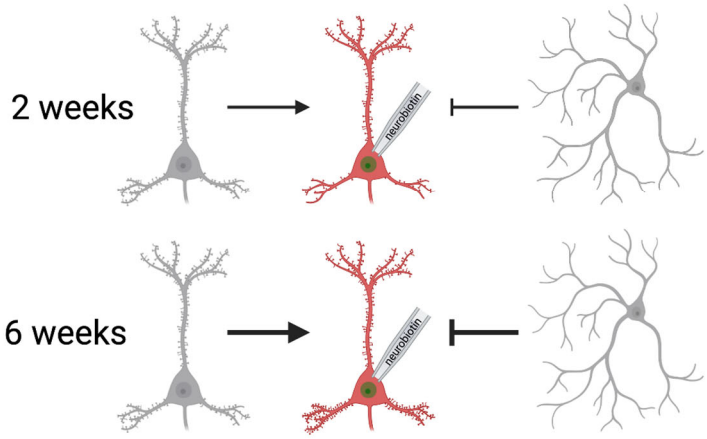

Figure 5. Inhibitory synaptic input to pyramidal neurons is increased after NMDAR ablation. (A) Sample traces of miniature inhibitory postsynaptic currents (mIPSCs) after 6 weeks of virus expression. **(B-C)** mIPSC amplitude is significantly increased in the Grin1 group (main effect of virus, $F_{1,27} = 5.350$, $P = 0.0286$), with no change in the cumulative probability distribution**. (D-E)** mIPSC amplitude is unchanged following NMDAR ablation (for B-E: control n/N = 15/5; Grin1 n/N = 16/4). Data are mean ± s.e.m. for all panels; open and closed circles indicate recordings from female and male mice, respectively. *P <0.05; two-way ANOVA (B, D); or Kolmogorov-Smirnov test (C, E); see Data S1 for complete statistics. **(F)** Summary table and figure **(G)** illustrating functional and structural changes over time following NMDAR ablation. https://BioRender.com/ilmaze5

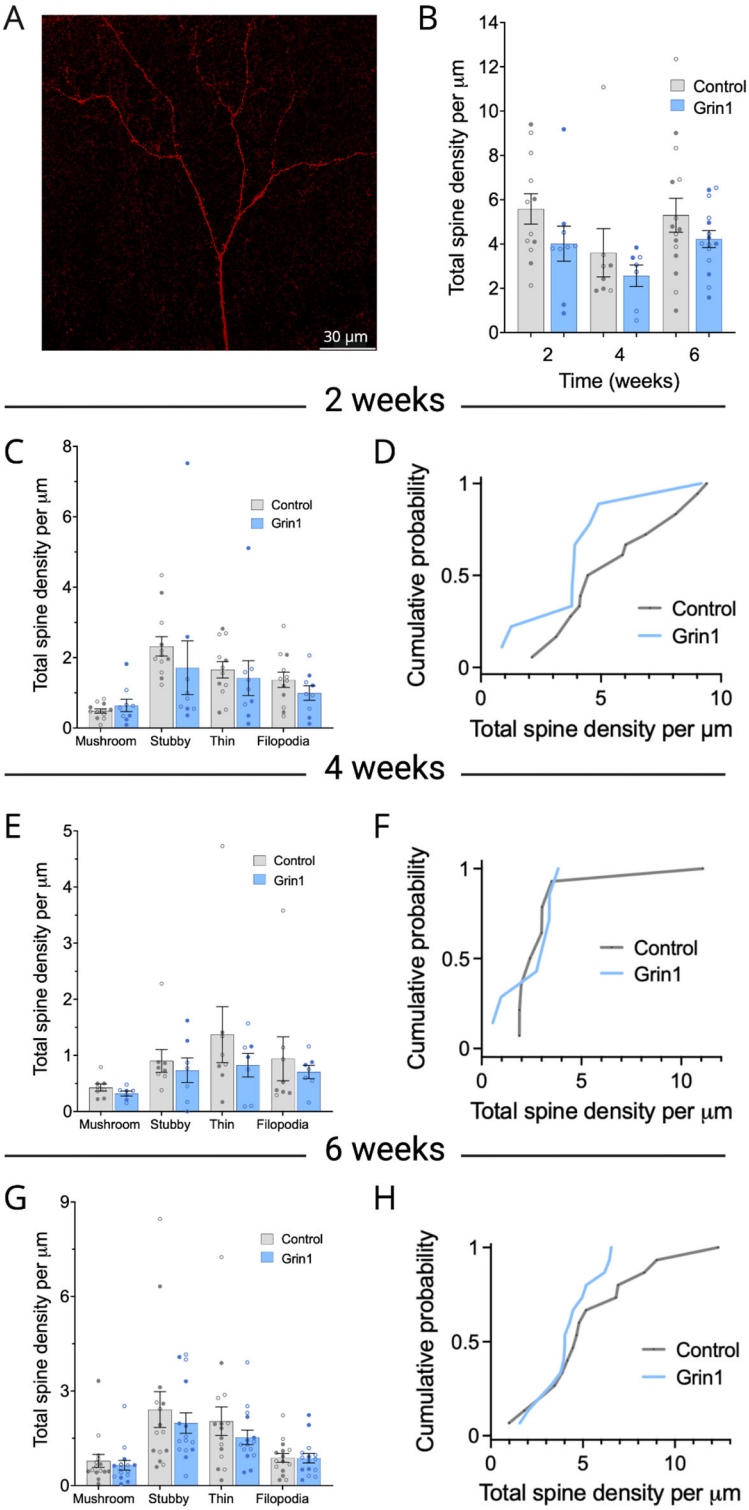

Figure S1. Apical spine density is unchanged following NMDAR ablation. (A) Sample image of the apical arbor of a layer V mPFC pyramidal neuron at 63x magnification. **(B)** No significant changes in total apical spine density in the Grin1 group at any timepoint (control n/N = 12/5, 8/6, and 15/8 for 2, 4, and 6 weeks; Grin1 n/N = 9/4, 7/4, and 15/9 for 2, 4, and 6 weeks). No significant change in apical spine density across all morphological categories and no difference in the cumulative probability distribution at two weeks **(C-D)**, four weeks **(E-F)**, or six weeks **(G-H)** (all sample sizes same as B). Data are mean ± s.e.m. for all panels; open and closed circles indicate recordings from female and male mice, respectively. Three-way ANOVA (B); two-way ANOVA (C, E, G); or Kolmogorov-Smirnov test (D, F, H); see Data S1 for complete statistics. https://BioRender.com/5cwkqrw